Photodesorption of NO from Au(100) using 3D surface-velocity map imaging

Saada Abujarada, [†a,b] *Huda AlSalem,* [†a,b] *Urslaan K. Chohan,* [c,d] *Gemma L. Draper,* [a,b] *Sven P. K. Koehler* [*a,b,c]

[a]School of Chemistry, The University of Manchester, Manchester M13 9PL, UK
[b]Photon Science Institute, The University of Manchester, Manchester M13 9PL, UK
[c]Dalton Cumbrian Facility, The University of Manchester, Moor Row CA24 3HA, UK
[d]School of Materials, The University of Manchester, Manchester M13 9PL, UK

Abstract

We measured the fully-resolved 3-dimensional velocity distributions of nitric oxide photodesorbed from a gold single crystal. These experiments combine time-of-flight measurements and the velocity map imaging technique to yield velocity distributions resolved in three dimensions for a prototypical surface-adsorbate system. Nitric oxide adsorbed on Au(100) was photodesorbed using a 355 nm laser beam. The desorbed NO molecules were ionised in the gas-phase by resonance-enhanced multi-photon ionisation within a set of velocity map imaging optics. The NO molecules preferentially leave the surface along the surface normal with a very narrow angular distribution, indicating a non-thermal desorption process.

Keywords: velocity map imaging, photodesorption, surface imaging, nitric oxide, DIET

[†]Both authors contributed equally to this work
*Corresponding author. Email: sven.koehler@manchester.ac.uk
The University of Manchester
School of Chemistry
Oxford Road
Manchester
M13 9PL
UK
+44 161 306 4448

1. Introduction

Studies of the detailed dynamics of chemical reactions frequently aim to record the product translational and/or internal energy distributions, both for gas-phase as well as for interfacial reactions, to learn about the energy re-distribution during the reaction, and ultimately about the reaction mechanism. The photo-induced desorption of fragments from a single crystal presents a well-defined reaction system due to the well-known surface structure and photon energy. The photon energy may be preserved to some extent in the gas-phase fragments whose internal and translational energy can be probed after leaving the surface, and can help to provide information about the dynamics of the desorption process.

A number of different experimental techniques have been employed in the past to study charged particle- and photon-induced desorption processes. Traditionally, one would use a time-of-flight (TOF) setup employing a mass-spectrometer that can be rotated around the fixed surface to acquire angularly-resolved translational energy distributions.[1] However, this is time-consuming (and lacks the internal energy distribution), hence in order to record all fragments simultaneously in a single experiment, imaging methods have risen in popularity. Winograd and co-workers have reported the energy- and angular-resolved distributions of neutrals (EARN) whose desorption was induced by ions, and they achieved an angular resolution of ~8°.[2,3] Similarly, ESDIAD (electron-stimulated desorption ion angular distributions) delivers angular distributions of ions desorbed from surfaces;[4] this method has successfully been employed for triangulation, i.e. it was in some cases possible to derive the orientations of molecular bonds at surfaces.[5]

State-resolved detection of neutrals typically involves the laser ionisation of neutral fragments, often performed in a resonance-enhanced multi-photon ionisation (REMPI) scheme. If a pump/desorption laser is employed to initiate an event at a surface, then laser-detection of neutrals a few mm above the surface can deliver kinetic energy distributions of fragments. However, unless an elaborate optical detection geometry is used, such kinetic energy distributions lack any angular information. Menges *et al*. demonstrated an elegant example of sheet-focussing of the ionisation laser (with the sheet perpendicular to the surface) to record two-dimensional velocity distributions state-selectively. This was done for the model system of NO photodesorbed from NiO, for which they obtained a bimodal velocity distribution, with most of the kinetic energy release being directed along the surface normal.[6]

A number of groups have recently adopted ion imaging techniques, which are heavily employed in gas-phase reaction dynamics,[7] to the study of surface dynamics. Briefly, ion imaging techniques in the gas-phase may be used to study e.g. photo-dissociation processes of small molecules; such molecules – seeded in a molecular beam – may be photo-dissociated and subsequently ionised within a set of ion optics which accelerate the ions down a TOF tube. Since the mass difference between the initially generated neutrals and the formed ions is negligible, the velocity of the neutrals expanding on a Newton sphere is preserved and can be re-constructed from the arrival position of the ions on a position-sensitive detector. Velocity-map imaging (VMI) was a technical improvement of ion imaging that ensured that the ions' arrival position is only a function of their velocity, and not of the position where they were formed.[8] Velocity resolutions of better than 1 % have been achieved in some VMI spectrometers.[9,10,11]

It hence seemed a logical step to adopt the VMI technique for surface studies in order to derive high-resolution velocity distributions. Wodtke and co-workers were the first to apply the VMI technique to surface desorption processes by combining VMI with TOF measurements.[12] In the laser-induced desorption of neutral Br atoms from a KBr single crystal, the surface of the crystal was oriented parallel to the ions optics and the detector, and the surface normal of the crystal was aligned along the TOF tube. TOF information – and hence velocity distributions along the surface normal – was obtained by varying the delay between the desorption and the ionisation laser, while VMI was used to derive the velocity distributions in the two dimensions parallel to the KBr surface. White and co-workers employed the surface-VMI technique to shed light onto the photodesorption of O_2 and photofragmentation of butanone adsorbed on $TiO_2(110)$.[13,14] Nesbitt and co-workers also employed surface-VMI to study molecular beam scattering of HCl from Au(100) single crystals;[15] most recently, they obtained 3D velocity information for HCl scattered from self-assembled monolayers by elegantly utilising the dc slicing technique to achieve a velocity resolution along the surface normal of around 11%.[16] In all of the above experiments, the surface normal was aligned along the TOF axis of the VMI spectrometer. In contrast, Harding *et al.* have recently demonstrated measurements of speed and angular distributions of N_2 scattered from a Au(111) single crystal whose surface normal lies in a plane parallel to the ion optics and detection plates.[17] Velocity distributions are in this case measured under spatial imaging conditions by varying the delay between ionization laser pulse and extraction pulse to follow the movement of the scattered molecules away from the surface, but parallel to the imaging detector.

The combination of TOF and VMI techniques can potentially produce fully-resolved three-dimensional velocity distributions of neutral fragments from surfaces; if REMPI spectroscopy is applied, internal state distributions can be obtained as well, i.e. fully-resolved internal and rotationally-resolved translational energy distributions can be recorded, the "holy grail" of reaction dynamics. However, for surface desorption processes, one has to pay attention to the exact geometry of the detection system: If the fragments are produced at one small spot on the surface and detected within a small volume above the surface, then some fragments may be missed, and hence the angular distribution measured is determined by this optical geometry, and may not reflect the dynamics of the process. Wodtke and co-workers overcame that problem by desorbing fragments from a relatively large spot on the surface, and ionising the neutral fragments within a small volume above the surface (referred to as *sheet-dot*), such that a relatively large polar angle of ~60° symmetric around the surface normal could be recorded.[12,18] We here present the first studies in which the more intuitive *dot-sheet* geometry is used to state-selectively record fully-resolved three-dimensional velocity distributions over almost the full 2π steradian; the experimental details, and the advantages and disadvantages of this approach are discussed in more detail in the experimental section.

The test system investigated here is the photodesorption of NO from a Au(100) single crystal. Nitric oxide is a key intermediate in a range of industrially-relevant processes, such as the reduction of higher oxidation state nitrogen compounds (nitrates and nitrites) to ammonium or ammonia compounds or laughing gas N_2O, as well as in the oxidation of ammonia.[19,20] On Pt surfaces, the exact pathway for ammonia reduction is still under dispute, not only regarding the intermediates, but also the mechanism, with both Langmuir-Hinshelwood as well as Eley-Rideal mechanisms being suggested.[19,21,22]

As for gold substrates, NO is more strongly adsorbed to Au(100) than to Au(111).[23] There is agreement that the nitrogen atoms face the gold surface, but there are conflicting report as to whether the neutral NO binds to Au(100) on the bridge site, i.e. between two neighboring atoms (2f site),[24] or the on-top (ot) site;[25] it is also disputed whether the NO is in a bent geometry,[25,26] or along the surface normal.[24] Temperature-programmed desorption experiments and density functional theory calculation agree that NO covalently binds to gold with an adsorption energy of ~57 kJ mol^{-1},[24] and adsorption at around ~170 K ensures sufficiently high coverages to induce a hex → (1×1) phase transition.[27]

While the photodesorption of nitric oxide from Au(100) has not been studied to date, NO is an attractive candidate as it is experimentally straightforwardly detected using REMPI spectroscopy.

Buntin *et al.* as well as Chuang and co-workers studied the laser-desorption of NO from Pt(111). Depending on the excitation wavelength, both found a bimodal velocity distribution, the faster component of which was attributed to excitation followed by electron-transfer to the NO adsorbate.[28,29,30] The desorption of NO from a non-metal Si(111) surface, however, has been found to be due to electronic excitations of the covalent substrate bonds.[31] So *et al.* investigated the interaction between laser radiation with NO adsorbed on GaAs(110) at 80 K over a range of wavelengths, and found that the desorption and dissociation of NO molecules are induced by non-thermal processes. The authors concluded that the observed desorption and dissociation could be attributed to interactions of the adsorbed NO with photogenerated charge carriers.[32] Menges *et al*. reported results on the angular distribution of NO desorbing from NiO(111) after excitation with 193 nm laser light using an experimental set-up capable of state-selectively obtaining the 2-dimensional velocity distribution of the desorbed neutrals in a single experiment.[6] Garcia *et al.* studied the photodissociation of NO adsorbed on Cu(110) using reflection-absorption infrared spectroscopy. The NO dimer was found to be photoactive in contrast to bridge-bonded NO which showed no photoactivity. NO dimers photodissociate by breaking the N-N bond, releasing one NO molecule to the gas phase, while the other NO remains adsorbed on the surface in the metastable atop position.[33]

We here report the application of 3D surface-velocity map imaging to the 355 nm photodesorption of NO from Au(100) surfaces. Section 2 describes in detail how we achieved to record the velocity distributions in three dimensions independently through a combination of TOF and VMI measurements. The results are presented in section 3, their analysis in section 4, followed by a discussion of the non-thermal nature of the NO desorption process.

2. Experimental

The experimental setup was designed to measure the velocity distribution of NO molecules photodesorbed from a Au(100) surface in three dimensions independently using a combination of TOF and VMI methods; the gas-phase VMI setup has been described in detail previously.[34] In brief, the spectrometer consists of two chambers, namely a molecular beam chamber which is only in operation when calibration experiments are performed, and a chamber that contains the Au(100) single crystal and the VMI optics . This chamber is evacuated by a 1000 L s^{-1} turbomolecular pump to achieve ultra-high vacuum conditions

(base pressure 5×10^{-10} Torr), backed by a mechanical pump. The VMI optics, described in more detail below, consist of twelve parallel plates of 10 cm diameter, the first of which, typically referred to as the repeller plate, features a 12 mm diameter central hole. A 10 mm diameter Au(100) crystal (1.5 mm thick) equipped with a K-type thermocouple is attached to a sample mount connected to a 3-axes/rotational manipulator which allows for heating and liquid nitrogen cooling, see Fig. 1.[35] While the 12 mm opening in the repeller plate can accommodate the Au crystal, physical contact between the liquid nitrogen-cooled crystal and the room-temperature repeller plate heats up the crystal too quickly, and the crystal is hence set-back by 0.5 mm behind (i.e. further away from the laser) and parallel to the repeller plate. The surface normal of the gold crystal is aligned along the TOF tube (*z* axis) of the spectrometer, at the end of which a 40 mm diameter multi-channel plate detector (Burle Photonis) is located (time-of-flight path for mass-separation is 45 cm). The manipulator also holds a 10 mm diameter stainless-steel disc with a central 2 mm hole; this disc can be placed in position instead of the gold crystal and allows us to run gas-phase calibration experiments using the molecular beam under otherwise identical conditions without having to break the vacuum. Both crystal and repeller plate are connected to separate power supplies held at the same voltage such that the field experienced by the fragments in vacuum at the point where they are ionised (between the repeller and the second plate) is homogenous, as proven by gas-phase calibration experiments.

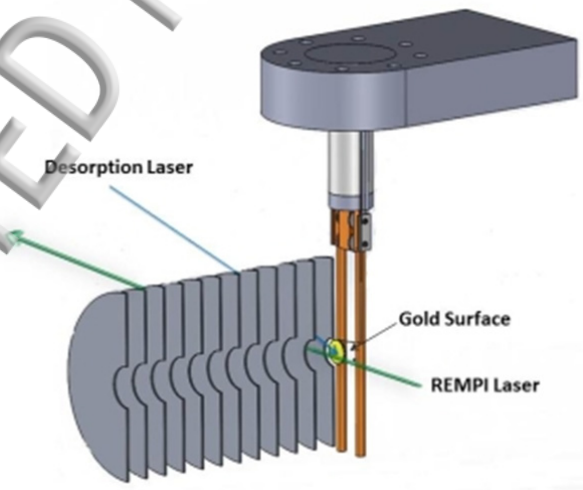

Fig. 1: Schematic of the 3D VMI setup showing the parallel alignment of the gold surface in relation to the ion optics.

The gold crystal is heated prior to experiments to 700 K and subsequently cooled to ~170 K. Nitric oxide (NO) gas is introduced into the chamber as background gas at a pressure of

~5×10^{-7} Torr for a few minutes, and the NO gas pressure is maintained at ~5×10^{-8} Torr during experiments to re-dose the surface, resulting in sub-monolayer NO coverage.[6,27] With the crystal in place, a frequency-tripled Nd:YAG laser (Quanta Ray DCR-11, $h\nu = 3.5$ eV, pulse duration 7 ns) beam is directed through small holes in the VMI electrodes at the NO/Au(100) surface at an angle of 45°. The energy of 1.5 mJ and the repetition rate of 20 Hz result in a transient temperature increase of ~27 K at the surface of the crystal.[36] This increase does not cause *thermal* desorption of NO molecules as shown later. The laser pulse nonetheless causes desorption of NO molecules which can potentially fly in all directions in the hemisphere above the surface. Since we are interested in the 3D velocity distribution, we have to ensure the capture of *all* NO molecules desorbing under all possible angles by paying particular attention to the optical detection geometry. If one was to desorb fragments from a small spot on the surface, and detect these fragments within a small volume above the surface, then the experiment is biased towards detecting only those fragments flying in a straight line from desorption spot on the surface to the detection volume. In order to detect all fragments, one can either increase the area which the desorption laser illuminates, and detect the fragments within a small volume above the surface (*sheet-dot*);[12,37] alternatively, one can use a small desorption laser spot on the surface (here ~2 mm diameter), and employ a detection laser sheet that ionises the NO fragments in a rather large volume above the surface (*dot-sheet*), see Fig. 2. Here, we report the latter, more-intuitive method for the first time. The NO molecules are ionised in a (1+1) REMPI scheme via the (0,0) A ← X transition; the third harmonic of a Continuum Powerlite 8020 Nd:YAG laser was used to pump a Radiant Dyes NarrowScan laser operating on Coumarin 460; the resulting output is frequency-doubled in a BBO crystal to yield ~200 μJ pulses at around 226 nm at 20 Hz. Employing the 8 mm diameter output from this laser system, we use a cylindrical lens with a focal length of 28 cm to create such a laser sheet above the surface. This yields an effective Rayleigh length z_R for 1+1 REMPI detection (keeping in mind that the ionisation step is saturated, and that the Rayleigh length for focusing with a cylindrical lens is defined by the beam dimension *in one direction* only doubling from waist to z_R) of more than 20 mm, hence effectively creating an 8 mm tall "curtain" above the surface through which the NO molecules have to fly. We note that we also translated the laser sheet up and down in front of the surface during measurements, but this did not affect the images, indicating that all NO radicals fly though the laser sheet. At a typical surface-to-laser distance of 3 mm, this allows us to detect all those NO molecules leaving the surface within a solid angle of 5.6 sr. As hinted above, the

This manuscript was accepted by J. Chem. Phys. Click here to see the version of record.

slightly more elaborate design of our ion optics consisting of twelve electrodes (yielding soft extraction conditions of around 50 V cm^{-1}) was chosen to increase the volume in which VMI conditions prevail, which we have previously established experimentally,[34] and we are hence confident that all NO molecules crossing the laser sheet are ionised and accelerated under true VMI conditions.

By varying the time delay between the desorption and the probe laser, we record time-of-flight profiles, but crucially, since the probe laser beam is focussed using a cylindrical lens and hence forms a sheet above the surface, these TOF profiles can be converted into velocity distributions that deliver the velocity component along the surface normal (v_z) exclusively, i.e. not the overall speed.

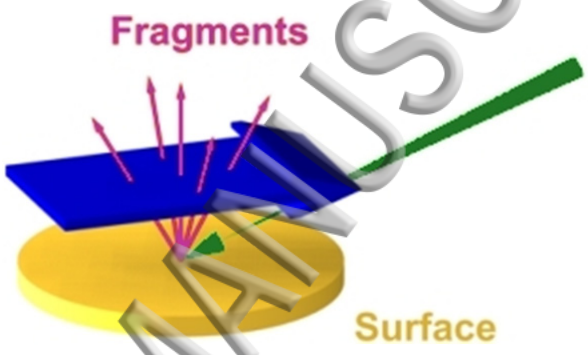

Fig. 2: Illustration of the dot-sheet conditions employed in this work. The photodesorption laser approaching from the right illuminates only a small area on the surface, while the probe laser forms a sheet above the surface to intersect as many desorbed molecules as possible.

An NO molecule desorbing from the surface straight along the surface normal ($v = v_z$) is detected by the REMPI laser after the same time delay as an NO molecule that leaves the surface with a certain angle and whose overall speed may be higher ($v > v_z$) as long as their velocity along z is the same; due to the "sheet"-shaped probe laser, converting these TOF profiles to velocity distributions hence delivers v_z. However, all particles ionised within this extended volume nonetheless adhere to velocity map imaging conditions as shown previously.[34] The ions are then accelerated down the time-of-flight tube (for mass separation) onto the position sensitive multi-channel plate (MCP) detector. This MCP detector is gated using a DEI PVX-4140 high voltage pulser in order to discriminate against ions other than NO^+. The ions' arrival positions are imaged onto a phosphor screen and captured by a synchronised CCD camera (FOculus FO124TB) before being transferred to a PC using a frame grabber (NI PCI- 8254R). Custom-written LabVIEW software is used to accumulate

and save the images, which are subsequently converted to velocity distributions. Since the gold surface and the detector are parallel to each other but perpendicular to the TOF axis of the spectrometer, the velocity distributions correspond to the remaining two velocity components v_x and v_y (where y is along the propagation direction of the REMPI laser, and x is the vertical axis in the laboratory frame, see Fig. 1) for specific values of v_z.
In essence, by varying the time delay between desorption and probe laser in discrete steps, we are able to record velocity distributions along z (v_z), and for each time delay, we obtain the velocity distribution along x and y from the velocity map images.

3. Results

Distributions of the NO velocity component flying along the z axis after 355 nm photodesorption were recorded by varying the delay time between the desorption and probe laser; such a TOF profile for a surface-to-REMPI laser distance of 3 mm is shown in Fig. 3a. Fig. 3b shows the velocity distribution v_z of NO molecules as an average of two runs; the time delays were now chosen to yield equally-spaced velocity intervals. However, since REMPI detection is sensitive to particle densities, and since each time delay probes a subset of NO molecules over a time interval determined by the probe laser pulse width (~7 ns), we applied the appropriate density-to-flux conversion and Jacobian.[38] These experiments were repeated with a surface-to-REMPI laser distance of 2 mm in order to record a larger solid angle of desorbing NO molecules (not shown), but this yielded the same result within the error of the experiment. The S/N ratio at 2 mm was comparable to that at 3 mm, indicating that we detected all NO molecules in both cases, but the velocity resolution along z at 2 mm is slightly worse such that all results reported here are for a 3 mm surface-to-REMPI laser distance unless otherwise stated. The error in the velocity distribution along the z axis is given by $\Delta l/l$, where Δl is the uncertainty of determining the exact distance between the surface and the probe laser; we estimate the error to be around 0.1 mm/3.0 mm = 3%. One major advantage of employing the TOF technique to acquire v_z with a well-defined laser-pump–laser-probe setup is the high velocity resolution obtained.

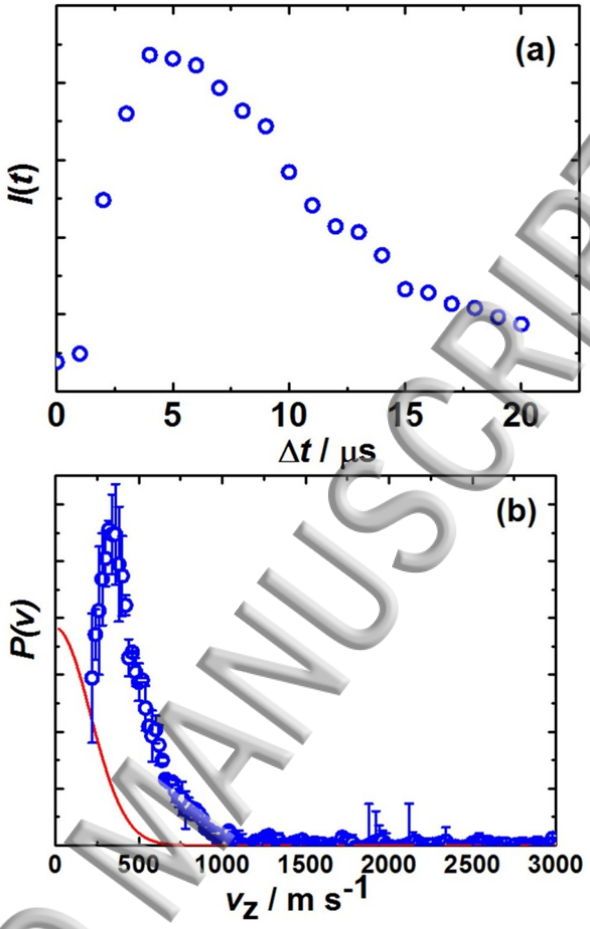

Fig. 3: (a) Raw time-of-flight data for NO photodesorbed from Au(100) at 355 nm. (b) v_z velocity distribution of photodesorbed NO after density-to-flux conversion of the raw data (blue circles), errors represent average of two runs. A 1D Maxwell-Boltzmann distribution at the surface temperature is provided for comparison (red line).

The remaining two velocity components v_x and v_y, which are parallel to the Au(100) surface, are derived from the velocity map images which are recorded at laser delay times corresponding to velocities v_z for which data points were recorded. These raw velocity map images, two of which are shown in Fig. 4, are recorded in density space and are subsequently converted to velocity space. Each raw image is composed of single images from approximately 20,000 laser shots. The center of these images corresponds to zero velocity in the *x* and *y* dimension, even though this center is shifted slightly with respect to the center of our CCD camera, an effect that we also observe to the same extent in our gas-phase experiments, and is due to the slight misalignment of the ion optics. The slight asymmetry we

observe in some images is also likely due to either the misalignment of the ion optics, and/or the round desorption laser illuminating an ellipsoidal area on the surface, and/or the probe laser, which is focussed using a cylindrical lens and has a Gaussian intensity profile in the direction not affected by the focussing; the latter favours fragments desorbing along the surface normal over those flying up or down in the laboratory frame, but fragments seem to intersect the central part of the laser beam, keeping distortions at a modest level.

In order to obtain three-dimensional velocity distributions, the results from the TOF profiles and the VM images must be appropriately combined as described in the next section.

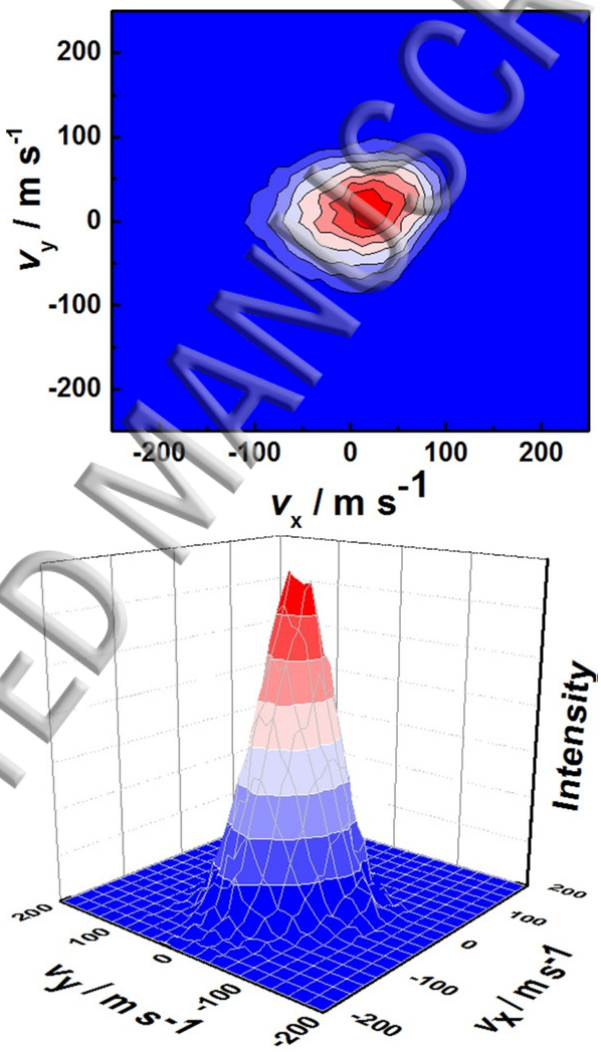

Fig. 4: Velocity map images of NO recorded at desorption-REMPI laser delay times corresponding to 420 m s^{-1} (top) and 560 m s^{-1} (bottom).

4. Discussion

Since the v_z distributions are strictly speaking 1D velocity distributions, they are compared in Fig. 3b with a 1D Maxwell-Boltzmann distribution at the temperature of the gold surface; however, the experimental v_z distribution of NO peaking at non-zero velocities is not well described by the 1D Maxwell-Boltzmann distribution, indicating a non-thermal desorption process. The experimental v_z distribution peaks at velocities just below 500 m s^{-1} and appears mono-modal.

Combining the TOF and VMI measurements results in 3D distributions which are cumbersome to visualize. Since the VM images appear roughly circular, i.e. there does not seem to be a preference for the NO molecules to fly along the [001] over the [010] direction, we azimuthally averaged the two velocity distributions parallel to the Au(100) surface to yield $v_{x/y}$. Fig. 5 shows a smoothed surface plot combining TOF data and VM images. It can be seen that while v_z is most intense at around 500 m s^{-1} and extends up to around 1000 m s^{-1}, $v_{x/y}$ almost completely vanishes at velocities higher than 200 m s^{-1}, illustrating that the desorption of NO molecules is confined to a rather narrow cone along the surface normal. To highlight this angular preference further, we created a polar contour plot of intensity as a function of both, overall speed and polar angle, see Fig. 6. The angular distribution is quite narrow throughout, always narrower than 25°, and it can be clearly seen that the NO molecules preferentially desorb along the surface normal. This is not unexpected, of course, as the flux of atoms or molecules leaving a surface typically peaks along the surface normal.[39,40] The smooth transition of the distributions from their peak along the surface normal to polar angles of only around 25° (i.e. without a sudden cut-off) also proves that we cover the full angular distribution which would theoretically, purely based on the detection geometry, have allowed detection of NO molecules up to polar angles of 53° (or even 63° for substrate-probe laser distances of 2 mm as used in some of the experiments here).

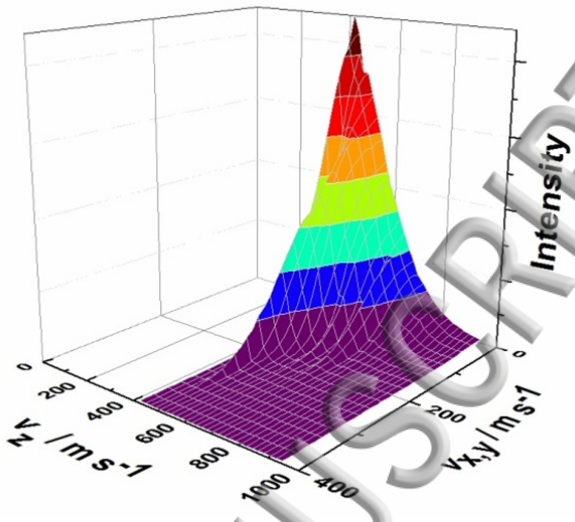

Fig. 5: Smoothed surface plot of NO flux as a function of v_z (from TOF measurements) and the azimuthally-averaged $v_{x/y}$ (from VM images) recorded at 3 mm surface-to-REMPI laser distances.

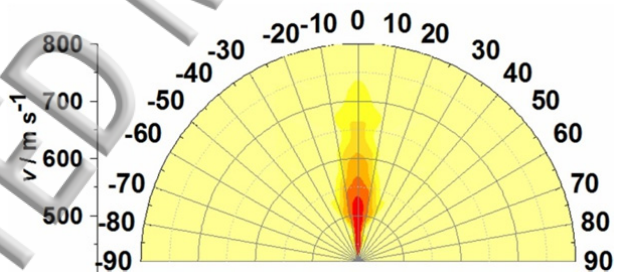

Fig. 6: Plot of the NO flux as a function of overall speed and angle after 355 nm photodesorption. Color scheme from red (most intense) to faint yellow (zero intensity). Note that the geometry of our 3D surface VMI setup allows NO molecules desorbing from the surface at angles of up to 53° to be detected.

Fig. 7 shows the angular distribution of the NO molecules for selected overall speeds. Also shown are fits of these distributions to $\cos^n \theta$ functions, where a fitting parameter of $n = 1$ is typical for thermal desorption processes. The angular distributions for even the slowest NO

molecules can only be fitted with $n > 1$, and it can also be seen that the angular distributions become narrower with increasing overall speed.

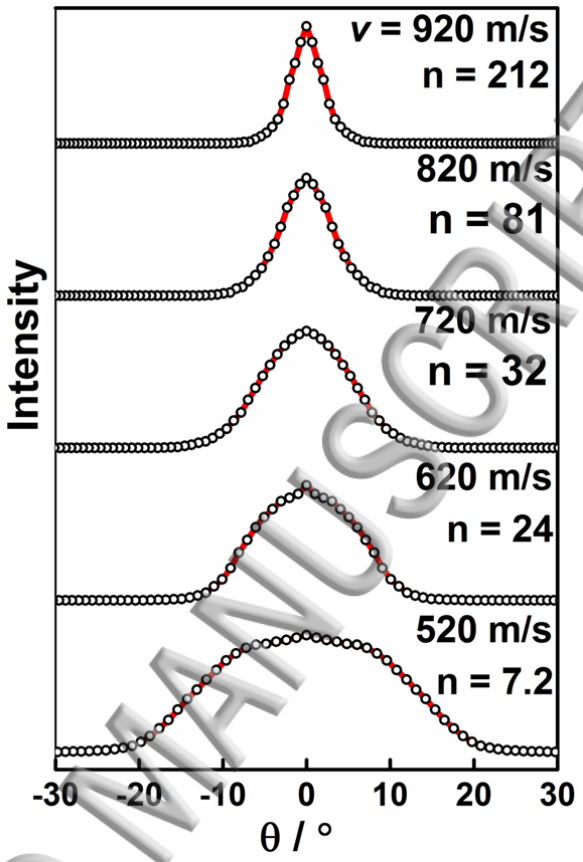

Fig. 7: Experimental angular distributions (circles) for selected speeds of photodesorbed NO molecules together with fits to a $\cos^n \theta$ distribution (red lines); plots are offset vertically for clarity.

Fig. 8 shows the overall speed distribution of NO molecules independent of angle, and compares it to a fitted 3D Maxwell-Boltzmann distribution at a temperature of 317 K. The lack of intensity below 400 m s^{-1} and the narrower distribution as compared to the Maxwell-Boltzmann fit are good indications that the overall speed distribution is not thermal. Fig. 9 shows the integrated (over all flight times) signal intensity of NO molecules desorbed from gold at various surface temperatures. It can be seen that a significant fraction of the NO molecules are still adsorbed to the surface even at and above the temperature reached during the laser pulse (~197 K), such that purely thermal desorption is unlikely to occur.

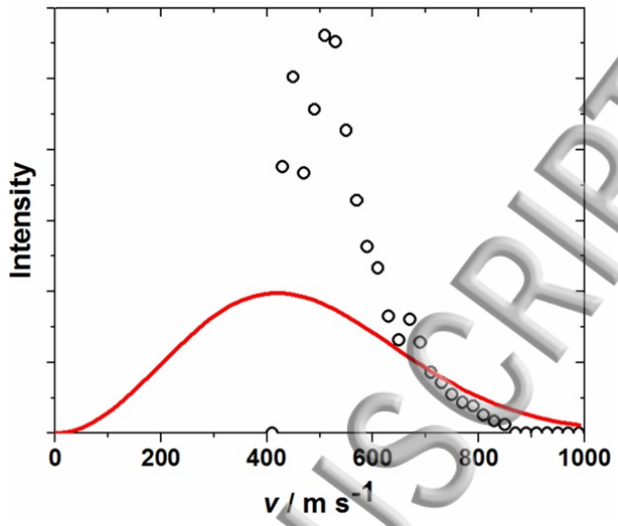

Fig. 8: Overall speed distribution of the desorbed NO molecules (obtained by appropriately combining v_z with v_x and v_y) and a Maxwell-Boltzmann best fit at a temperature of 317 K in red.

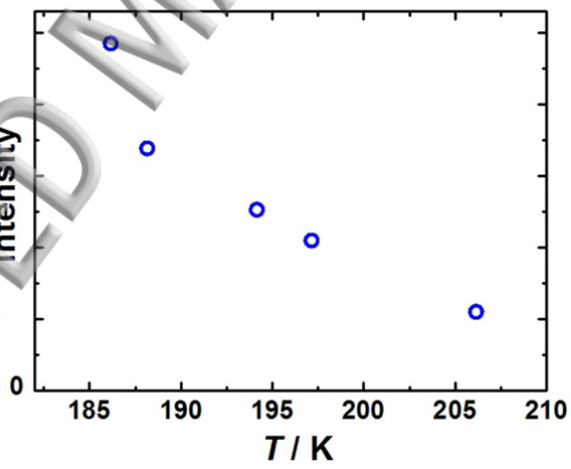

Fig. 9: Integrated signal intensity of NO desorbed from Au(100) as a function of temperature.

All the above results point to a non-thermal mechanism due to electronic excitation. This could either be a "hot" electron mechanism in which an electron from the conduction band is excited above the Fermi level (E_f); this is followed by tunnelling into an unoccupied state of the adsorbate forming a negative ionic state, from which desorption of the neutrals occurs.[41,42] Fukutani *et al.* consider such a mechanism for the 193 nm photodesorption of NO

from Pt(111).[30] Alternatively, the photon may cause excitation within the adsorbate molecule which – once in an excited state – undergoes desorption. For NO on Ni(111), Yates and co-workers argue that the interaction between the NO $2\pi^*$ antibonding orbital and the Ni d bands causes the occupied NO $2\pi^*$-d state and the unoccupied NO $2\pi^*$-d state to be below and above the Fermi level with an energy gap of ~3.7 eV, close to the excitation laser wavelength of 355 nm used in their experiments.[43] Rogozik *et al.* reported that these levels are expected to broaden and extend to near E_f as a result of the strong molecule/metal interaction.[44] It seems hence plausible that the desorption of NO from Au(100) observed in this work at 355 nm is also either due to excitation within the adsorbed NO itself, or due to a substrate-mediated mechanism.

In order to shed more light onto the excitation mechanism of NO adsorbed on Au(100), we performed first principles quantum chemical calculations based on density-functional theory. We employed the Cambridge Serial Total Energy Package (CASTEP) which solves the Kohn-Sham equations with a plane wave basis set employing three-dimensional periodic boundary conditions,[45] similar to our previous work.[46] We used the Perdew–Burke–Ernzerhof (PBE) functional to approximate the exchange and correlation effects in the electronic properties.[47] For all but 100% coverage, we find that the NO preferentially adsorbs on the bridge (2f) site with a weak adsorption energy of between 0.65 eV and 0.8 eV depending on coverage. This is roughly in agreement with previous calculations by Olvera-Neria *et al.* (0.53 eV) for NO on a single gold atom,[48] and by Niemantsverdriet and co-workers (0.57 eV for adsorption on the bridge site)[24] Thermal desorption experiments (0.59 eV) also agree with the above calculated adsorption energies,[27] but are in contrast to Liu and co-workers who computationally studied 25% coverage of NO on Au(100) and found an adsorption energy of 0.26 eV for the on-top (ot) site;[25] we note that we calculate an adsorption energy of 0.20 eV for the ot site, but – as mentioned above – also find an energetically more favourable conformation in the form of the 2f site. On the latter, the single electron in the two NO π^* orbitals (belonging to the nitrogen atom) can efficiently overlap with the orbitals on two neighbouring Au atoms at the surface between which the NO is located, resulting in an N-O bond aligned along the surface normal. We find this upright arrangement in fact for all sites and coverages apart from on-top cases, where overlap of the π^* orbital with the orbitals on a single Au atom causes the NO to tilt.

We mapped the partial density-of-states of the Au-NO complex around the Fermi energy separately for the Au atom and the NO molecule in search for a plausible non-thermal

excitation mechanism. It appears that for the 2f site (as well as for the hollow 4f, but not for the ot site), some filled Au orbitals (belonging to p orbitals) at ~3 eV below the Fermi energy, and some unoccupied orbitals belonging to the nitrogen p orbitals of the NO around 0.5 eV above the Fermi energy, exist. Since this gap of ~3.5 eV is roughly equivalent to our excitation laser wavelength of 355 nm, excitation from the substrate to the adsorbate is likely to be responsible for the non-thermal desorption of NO from Au(100).

5. Conclusions

In this paper, we have demonstrated the capability of a 3D surface VMI apparatus to study photodesorption processes. The combination of TOF and imaging methods negates the need for complex instrumentation employing rotatable mass-spectrometers for which data acquisition can be time-consuming. 3D surface VMI delivers fully-resolved velocity distributions with high resolution if one ensures that all desorbing particles are detected, and presents hence a faster method for surface reaction studies. The angularly-resolved velocity distributions of NO photodesorbed from Au(100) indicate that a non-thermal mechanism is responsible for NO desorption, and this seems likely to be induced by a substrate-mediated excitation.

ACKNOWLDGEMENTS

We thank the Dalton Cumbrian Facility program in part funded by the Nuclear Decommissioning Authority for funding; HAS and SA thank the Saudi and Libyan government, respectively, for funding. We also thank Alisdair Macpherson for help with the Quanta Ray laser system.

[1] S. T. Ceyer, G. A. Somorjai, *Ann. Rev. Phys. Chem.* **28**, 477 (1977).
[2] P. H. Kobrin, G. A. Schick, J. P. Baxter, N. Winograd, *Rev. Sci. Instrum.* **57**, 1354 (1986).
[3] S.W. Rosencrance, D.E. Riederer, R. Chatterjee, C. He, N. Winograd, Z. Postawa, *Nucl. Instrum. Meth. Phys. Res. B*, **101**, 137 (1995).
[4] J. J. Czyzewski, T. E. Madey, J.T. Yates, Jr., *Phys. Rev. Lett.* **32**, 777 (1974).
[5] J.-G. Lee, J. Ahner, J. T. Yates, Jr., *J. Am. Chem. Soc.* **124**, 2772 (2002).
[6] M. Menges, B. Baumeister, K. Al-Shamery, H.-J. Freund, C. Fischer, P. Andresen, *Surf. Sci.* **316**, 103 (1994).
[7] D. W. Chandler, P. L. Houston, *J. Chem. Phys.* **87**, 1445 (1987).
[8] A. T. J. B. Eppink, D. H. Parker, *Rev. Sci. Instrum.* **68**, 3477 (1997).
[9] W. Li, S. D. Chambreau, S. A. Lahankar, A. G. Suits, *Rev. Sci. Instrum.* **76**, 063106 (2005).
[10] G. Wu, W. Zhank, H. Pan, Q. Shuai, B. Jiang, D. Dai, X. Yang, *Rev. Sci. Instrum.* **79**, 094104 (2008).
[11] J. J. Lin, J. Zhou, W. Shiu, K. Liu, *Rev. Sci. Instrum.* **74**, 2495 (2003).
[12] S. P. K. Koehler, Y. Ji, D. J. Auerbach, A. M. Wodtke, Phys. Chem. Chem. Phys. 11, 7540 (2009).
[13] D. Sporleder, D. P. Wilson, M. G. White, *J. Phys. Chem. C* **113**, 13180 (2009).

[14] M. D. Kershis, D. P. Wilson, M. G. White, J. J. John, A. Nomerotski, M. Brouard, J. W. L. Lee, C. Vallance, R. Turchetta, *J. Chem. Phys.* **139**, 084202 (2013).
[15] J. R. Roscioli, D. J. Bell, D. J. Nelson, D. J. Nesbitt, *Phys. Chem. Chem. Phys.* **14**, 4070 (2012).
[16] C. H. Hoffman, D. J. Nesbitt, *J. Phys. Chem. C* **120**, 16687 (2016).
[17] D. J. Harding, J. Neugebohren, D. J. Auerbach, T. N. Kitsopoulos, A. M. Wodtke, *J. Phys. Chem. A* **119**, 12255 (2015).
[18] Y. Ji, S. P. K. Koehler, D. J. Auerbach, A. M. Wodtke, *J. Vac. Sci. Technol. A* **28**, 807 (2010).
[19] S. Horold, K.-D. Vorlop, T. Tacke, M. Sell, *Catal. Today* **17**, 21 (1993).
[20] V. Rosca, G. L. Beltramo, M. T. M. Koper, *Langmuir **21**,* 1448 (2005).
[21] A. Cuesta, M. Escudero, *Phys. Chem. Chem. Phys.* **10**, 3628 (2008).
[22] A. Clayborne, H.-J. Chun, R. B. Rankin, J. Greeley, *Angew. Chem. Int. Ed.* **54**, 8255 (2015).
[23] S. A. C. Carabineiro, B. E. Nieuwenhuys, *Gold Bull.* **42**, 288 (2009).
[24] A. Hussain, D. Curulla Ferré, J. Gracia, B.E. Nieuwenhuys, J.W. Niemantsverdriet, *Surf. Sci.* **603**, 2734 (2009).
[25] Y. Wang, D. Zhang, C. Liu, *Sci. China Chem.* **54**, 194 (2011).
[26] O. Olvera-Neria, V. Bertin, E. Poulain, *Intern. J. Quant. Chem.* **111**, 2054 (2011).
[27] E.D.L. Rienks, G.P. van Berkel, J.W. Bakker, B.E. Nieuwenhuys, *Surf. Sci.* **571**, 187 (2004).
[28] S. A. Buntin, L. J. Richter, D. S. King, R. R. Cavanagh, J. Chem. Phys. **91**, 6429 (1989).
[29] R. Schwarzwald, A. Mödl, T. J. Chuang, *Surf. Sci.* **242**, 437 (1991).
[30] K. Fukutani, Y. Murata, R. Schwarzwald, T. J. Chuang, *Surf. Sci.* **311**, 247 (1994).
[31] L. J. Richter, S. A. Buntin, D. S. King, R. R. Cavanagh in *Desorption Induced by Electronic Transitions DIET V*, Vol. 31, Springer Series in Surface Sciences, pp 227-232.
[32] S. K. So, W.Ho, Appl. Phys. A 47, 213 (1988).
[33] N. Garcia Rey, H. Arnolds, *J Chem. Phys.* **135**, 224708 (2011).
[34] M. Reid, S. P. K. Koehler, Rev. Sci. Instrum. 84, 044101 (2013).
[35] J. Ahner, D. Mocuta, R. D. Ramsier, J. T. Yates, Jr., *J. Chem. Phys.* **105**, 6553 (1996)
[36] J. H. Bechtel, *J. Appl. Phys.* **46**, 1585 (1975).
[37] D. A. Chestakov, S. M. Wu, G. R. Wu, D. H. Parker, A. T. J. B. Eppink, T. N. Kitsopoulos, *J. Phys. Chem. A* **108**, 8100 (2004).
[38] I. Rahinov, R. Cooper, C. Yuan, X. Yang, D. J. Auerbach, A. M. Wodtke, J. Chem. Phys. **129**, 214708 (2008).
[39] O. J. Maselli, J. R. Gascooke, W. D. Lawrance, M. A. Buntine, *Chem. Phys. Lett.* **513**, 1 (2011).
[40] G. Comsa, R. David, *Surf. Sci. Rep.* **5**, 145 (1985).
[41] P.R. Antoniewicz, Phys. Rev. B 21, 3811 (1980).
[42] J.W. Gadzuk, L.J. Richter, S.A. Buntin, D.S. King, R.R. Cavanagh, Surf. Sci. 235, 317 (1990).
[43] J. Yoshinobu, X. Guo, J. T. Yates Jr., *J. Chem. Phys.* **92** 7700 (1990).
[44] J. Rogozik, J. Kiippers, V. Dose, *Surf. Sci.* **148**, L653 (1984).
[45] S. J. Clark, I. Matthew, D. Segall, C. J. Pickard, P. J. Hasnip, M. I. J. Probert, K. Refson, M. C. Payne, Z. Kristallogr. **220**, 567 (2005).
[46] U. K. Chohan, E. Jimenez-Melero, S. P.K. Koehler, *Appl. Surf. Sci.* **387**, 385 (2016).
[47] J.P. Perdew, K. Burke, M. Ernzerhof, *Phys. Rev. Lett.* **77**, 3865 (1996).
[48] O. Olvera-Neria, V. Bertin, E. Poulain, *Intern. J. Quant. Chem.* **111**, 2054 (2011).

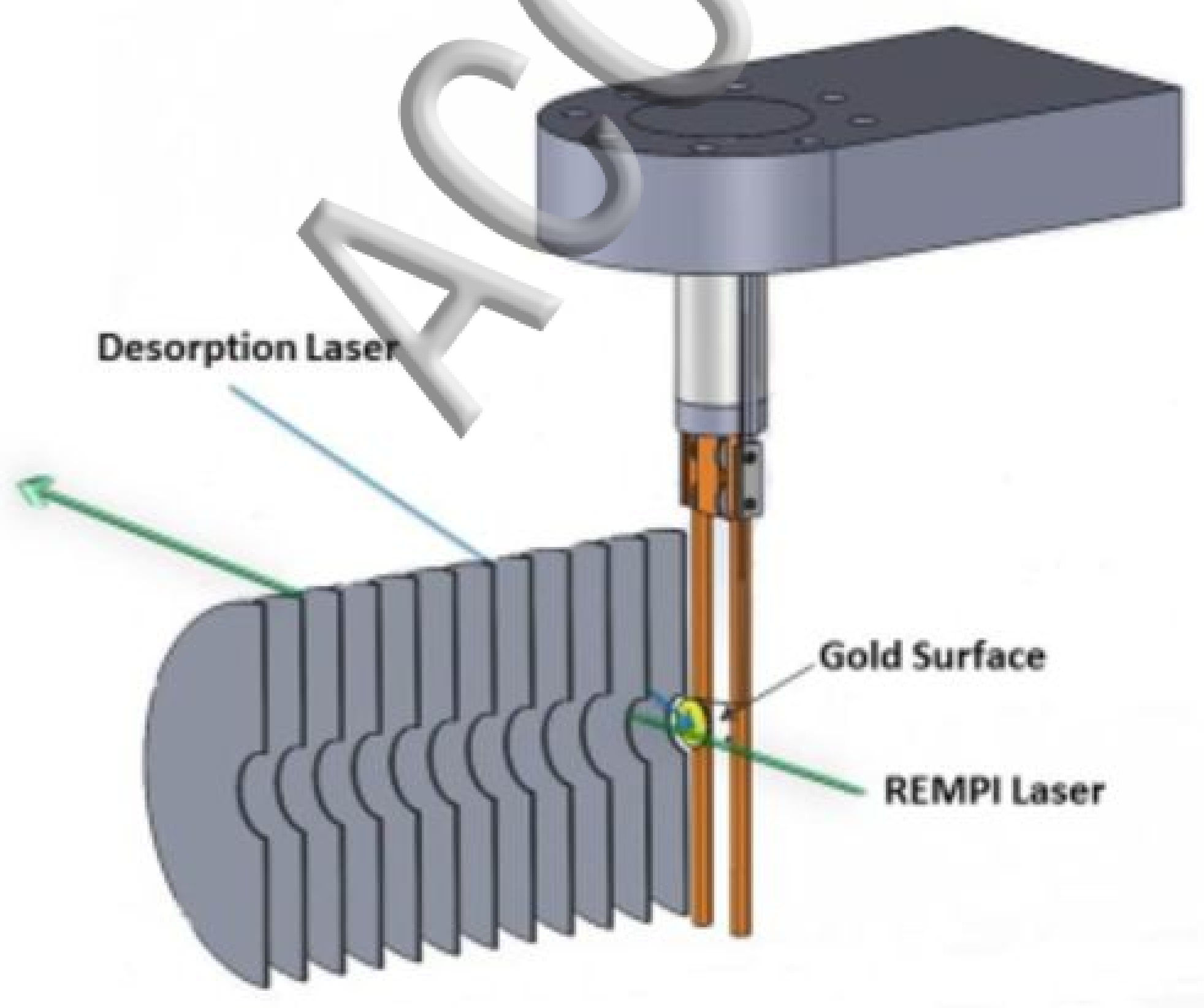
Desorption Laser
Gold Surface
REMPI Laser

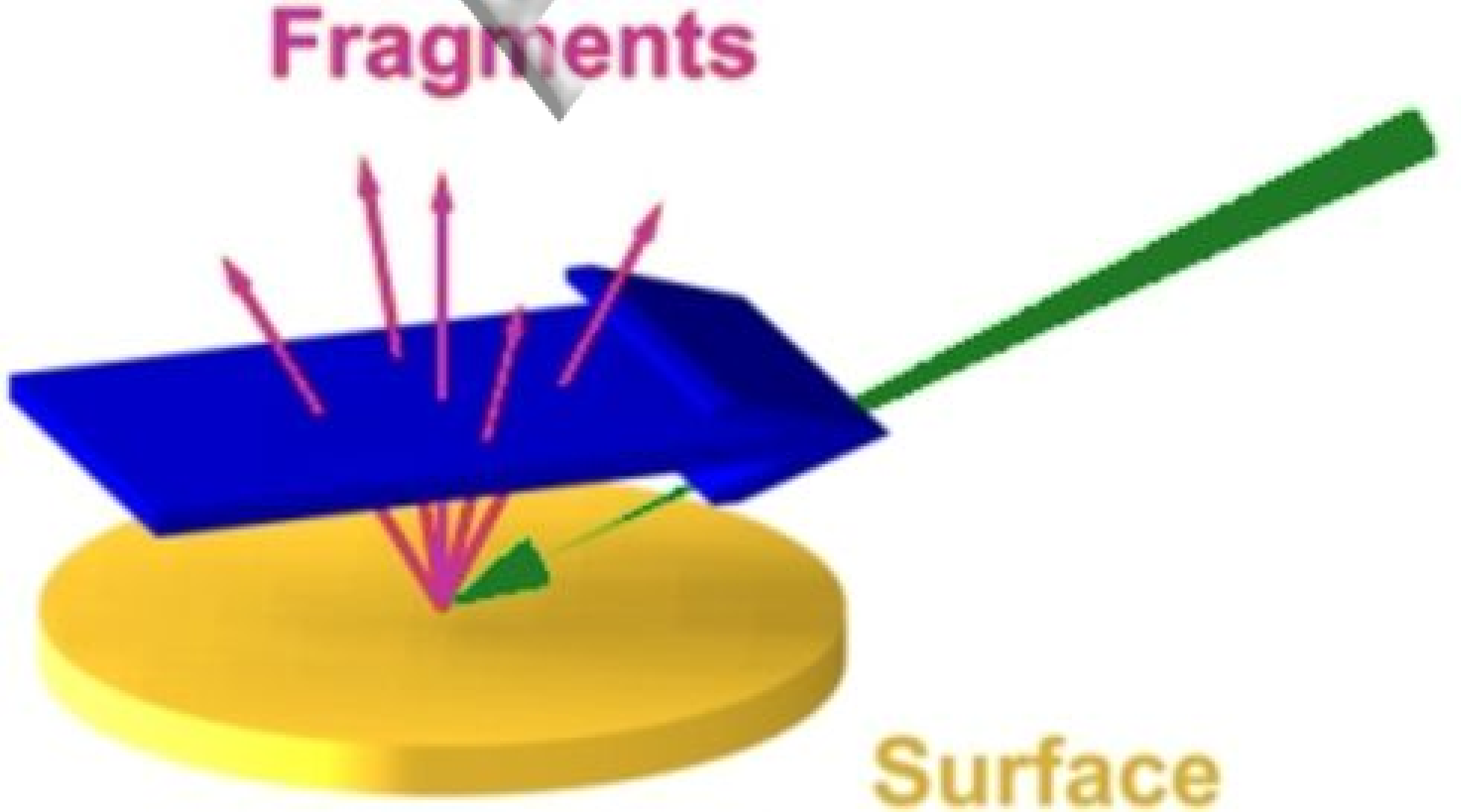
Fragments
Surface

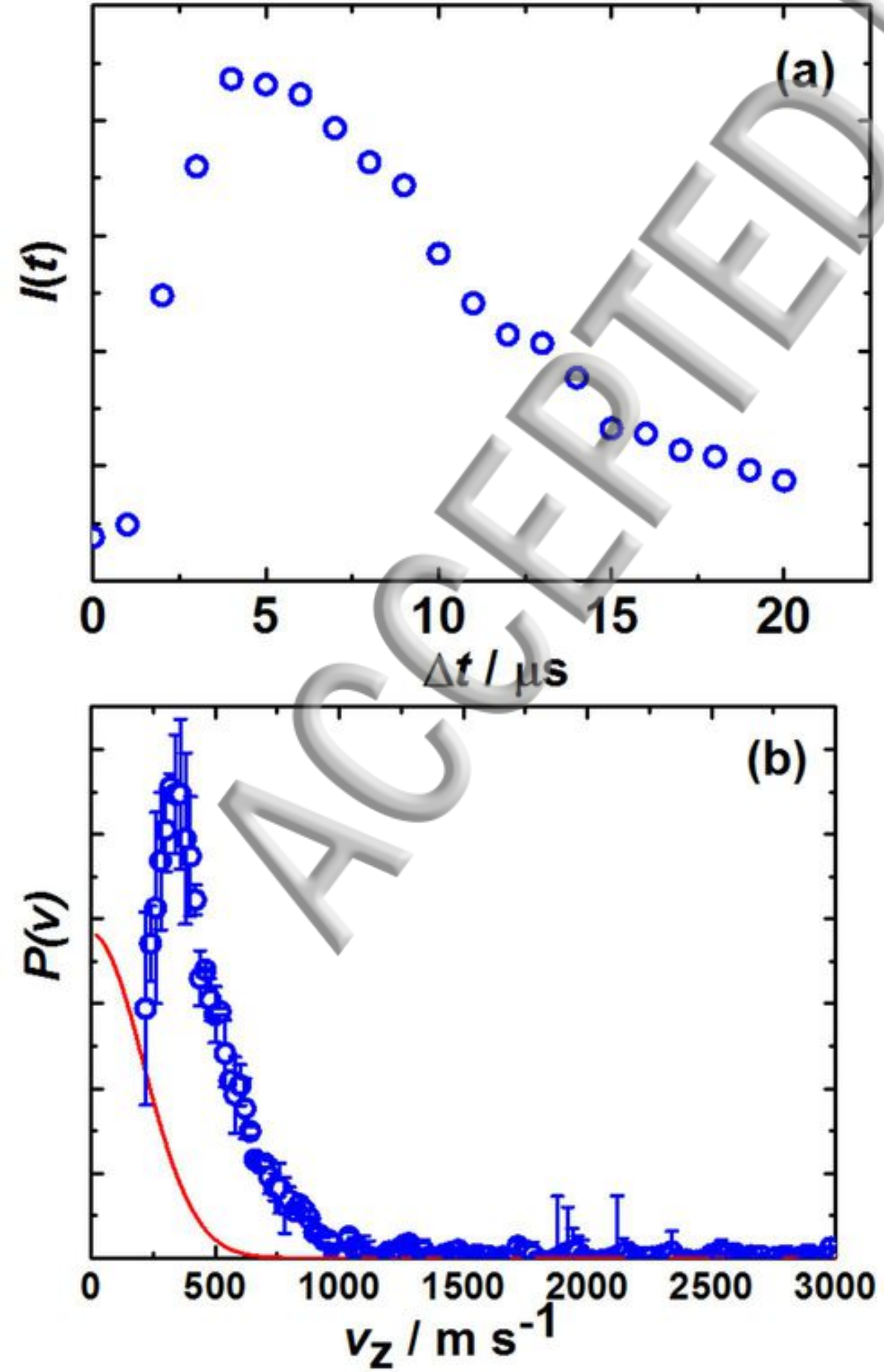

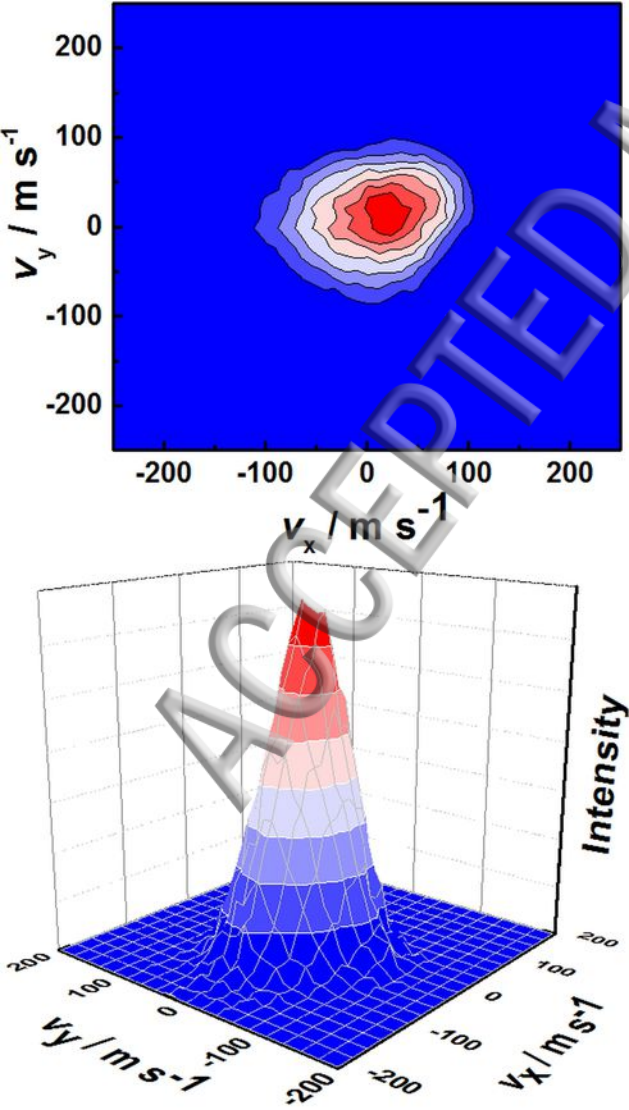
200
100
0
-100
-200
v_y / m s^{-1}
-200
-100
0
100
200
v_x / m s^{-1}
Intensity
200
100
0
-100
-200
v_y / m s^{-1}
200
100
0
-100
-200
v_x / m s^{-1}

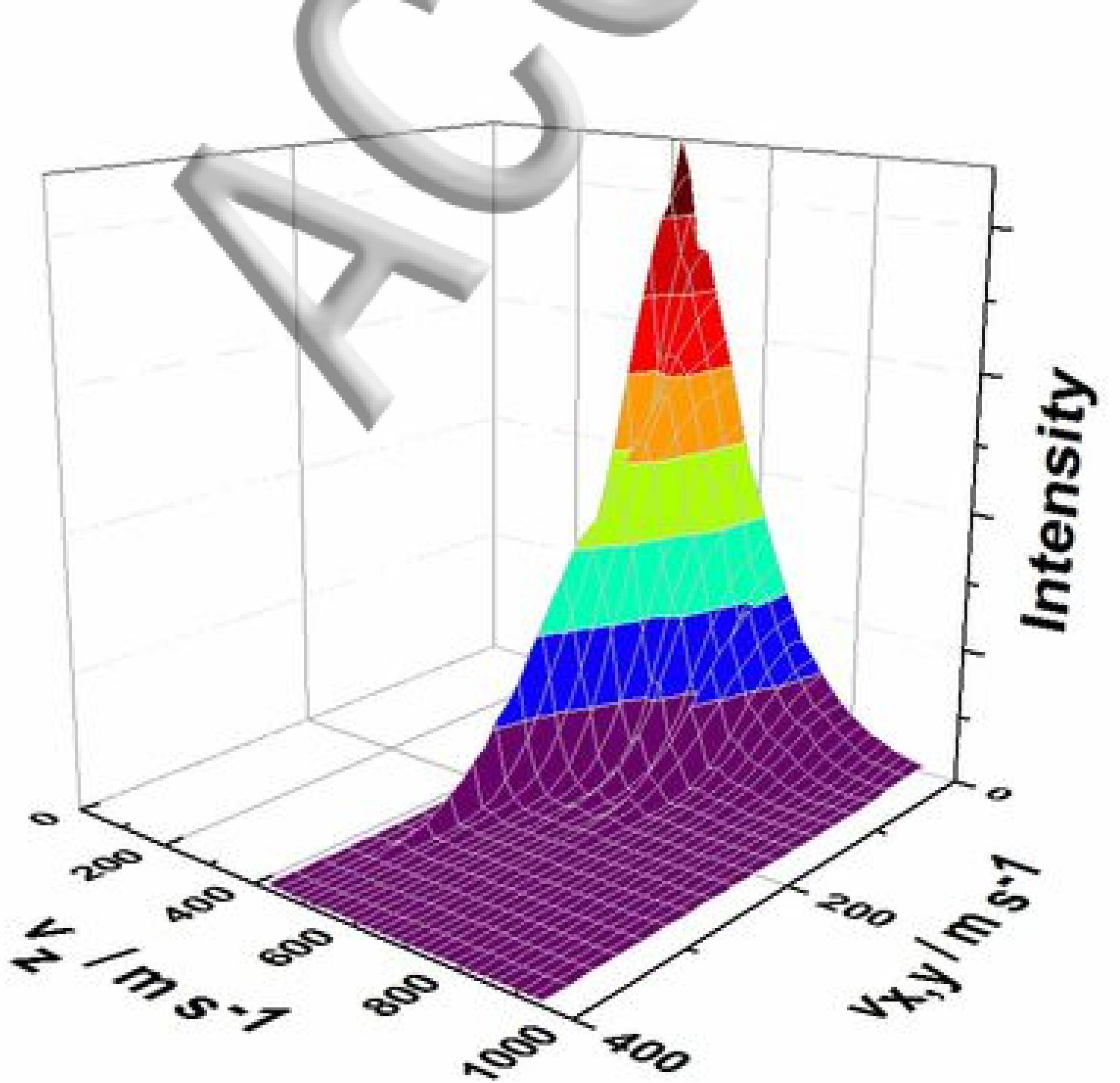
Intensity
0
200
400
600
800
1000
Vz / m s-1
400
200
0
Vx,y / m s-1

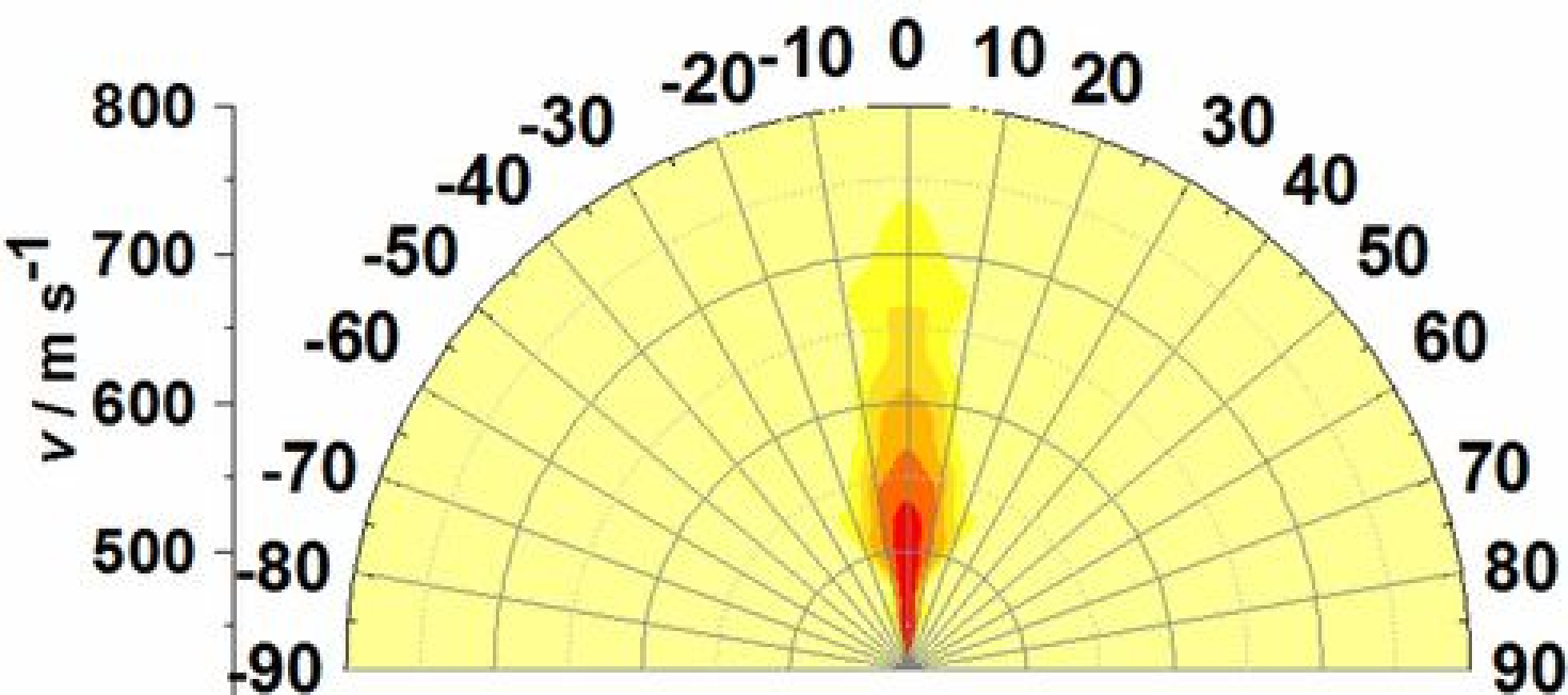
v / m s-1
800
700
600
500
-90
-80
-70
-60
-50
-40
-30
-20
-10
0
10
20
30
40
50
60
70
80
90

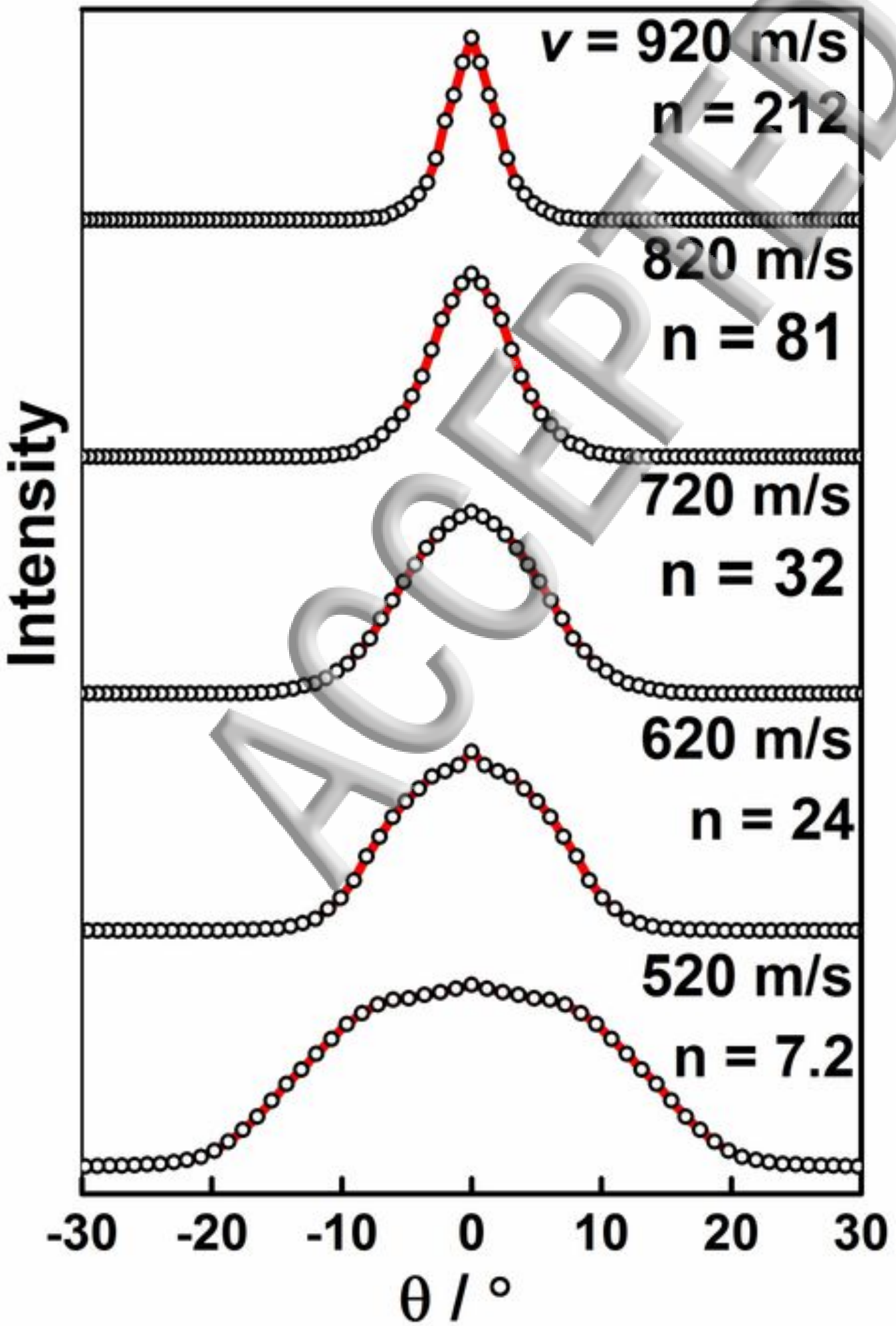
v = 920 m/s
n = 212
820 m/s
n = 81
720 m/s
n = 32
620 m/s
n = 24
520 m/s
n = 7.2
Intensity
-30
-20
-10
0
10
20
30
θ / °

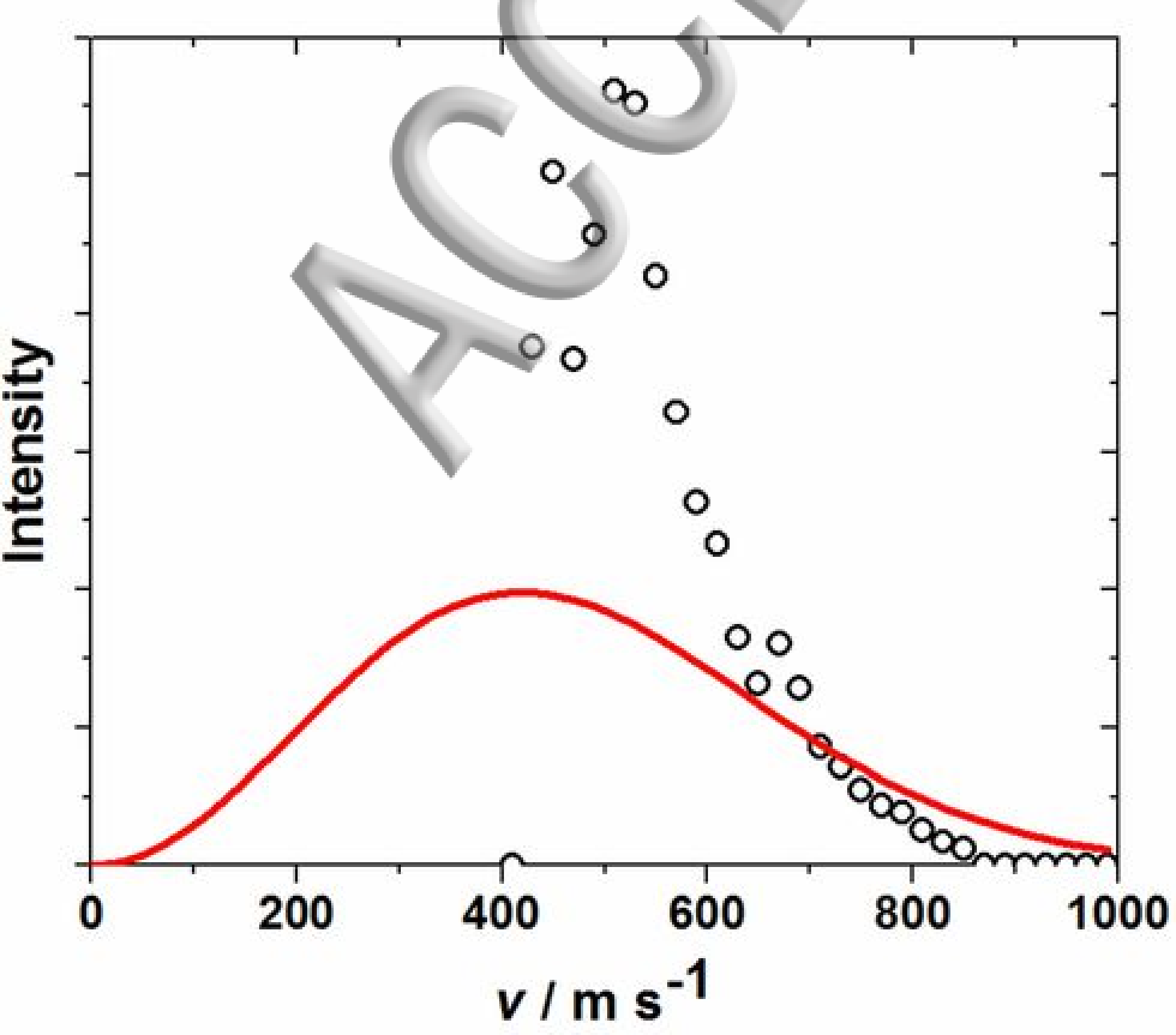
Intensity
0
200
400
600
800
1000
v / m s-1

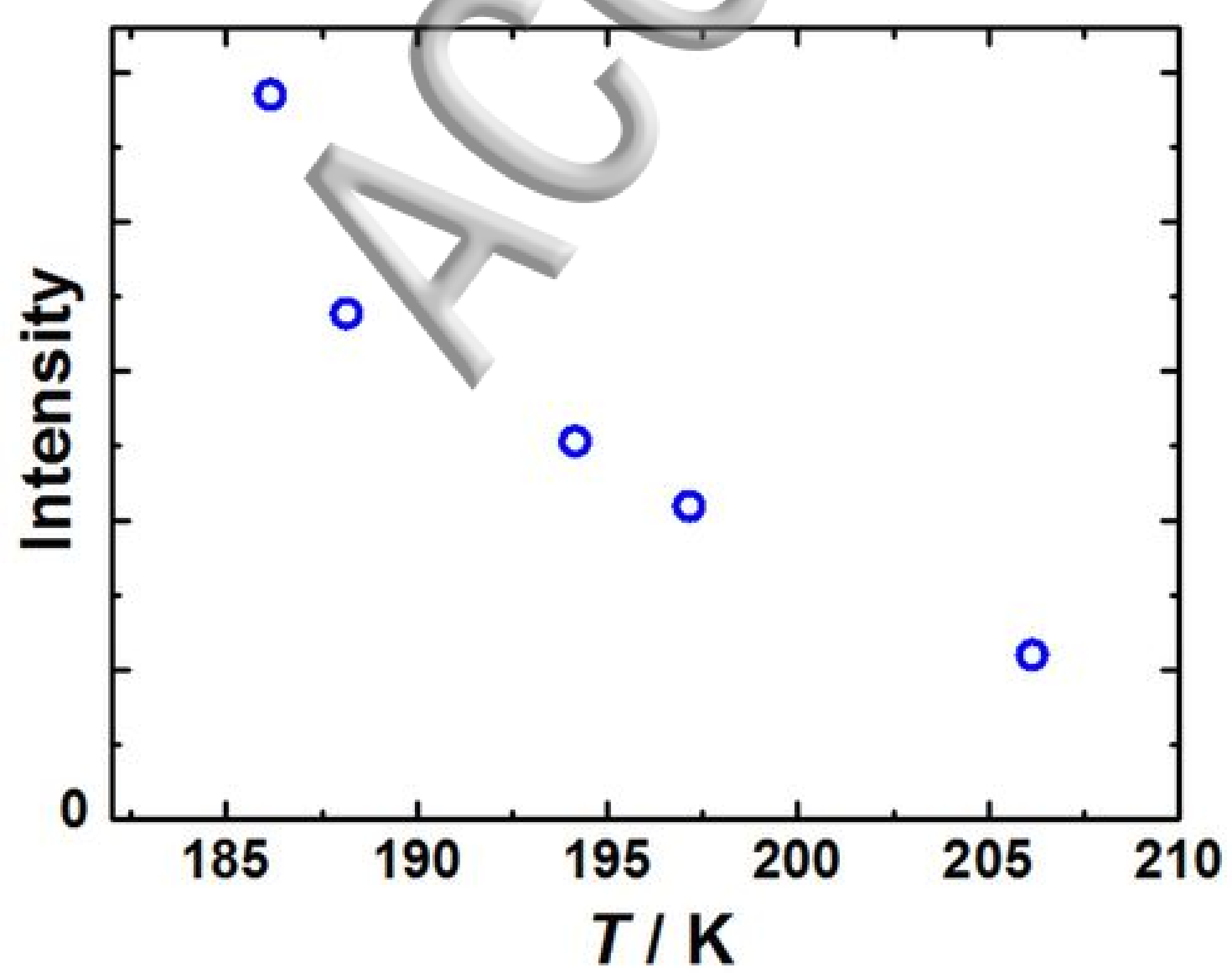
Intensity
0
185
190
195
200
205
210
T / K